Evidence of Fermi level pinning at the Dirac point in epitaxial multilayer graphene

S. Massabeau, Matthieu Baillergeau, T. Phuphachong, C. Berger, W. A. de Heer, S. Dhillon, J. Tignon, L. A. de Vaulchier, R. Ferreira, J. Mangeney

HAL Id: hal-01542964

https://hal.science/hal-01542964

Submitted on 20 Jun 2017

Evidence of Fermi level pinning at the Dirac point in epitaxial multilayer graphene

S. Massabeau,[1] M. Baillergeau,[1] T. Phuphachong,[1] C. Berger,[2,3] W. A. de Heer,[2,4] S. Dhillon,[1]
J. Tignon,[1] L. A. de Vaulchier,[1] R. Ferreira,[1] and J. Mangeney[1]

[1]*Laboratoire Pierre Aigrain (LPA), Ecole normale supérieure, Paris Sciences et Lettres (PSL) Research University,*
Centre national de la recherche scientifique (CNRS), Université Pierre et Marie Curie,
Sorbonne Universités, Université Paris Diderot, Sorbonne Paris-Cité, 24 rue Lhomond, 75231 Paris Cedex 05, France
[2]*School of Physics, Georgia Institute of Technology, Atlanta, Georgia 30332, USA*
[3]*Université Grenoble Alpes/CNRS, Institut Néel, Grenoble, 38042, France*
[4]*Tianjin International Center for Nanoparticles and Nanosystems, Tianjin University, China*

We investigate the temperature-dependent conductivity of epitaxial multilayer graphene using THz time-domain spectroscopy and find evidence that the Fermi level in quasineutral graphene layers is pinned at the Dirac point by midgap states. We demonstrate that the scattering mechanisms result from the interplay between midgap states that dominate in the vicinity of the Dirac point and short-range potentials that govern at higher energies (>8 meV). Our results highlight the potential of multilayer epitaxial graphene for probing low-energy Dirac particles and also for THz optics.

I. INTRODUCTION

Graphene provides an ideal two-dimensional system of quasirelativistic massless Dirac fermions. Its unusual properties have led to demonstrations of many intriguing fundamental physic phenomena as well as advanced devices for various applications such as high-frequency electronics. Owing to its zero bandgap, graphene is also interesting for fundamental study of interband processes at THz frequencies. In addition, these processes are highly desired for the technological development of THz photonic devices [1]. However, this requires large graphene crystal with extremely low Fermi level energy ($\leqslant 2$ meV) since interband processes are allowed only from energies higher than 2 E_F [2].

Epitaxial growth of graphene on C-terminated surface of 4H-SiC substrate is very promising since it yields a high-quality multilayer graphene at the wafer scale on flat, noninteracting and semiconducting substrate [3]. Multilayer epitaxial graphene (MEG) includes many independent quasineutral layers (owing to the layer rotational stacking [4]) with Fermi level energy that has been previously inferred to be less than 7 meV [5,6]. Also, up to 100 quasineutral layers can be stacked in MEG, resulting in very strong optical absorption [7]. However, how close the Fermi level is to the Dirac point in the quasineutral layers remains to be elucidated. The investigation of the quasineutral layers in MEG at very low energies is difficult. Indeed, directly probing the quasineutral layers using transport experiments [3,8] is prevented owing to the presence of few highly-doped layers near the substrate interface [6]. In addition, conventional magneto- and infrared spectroscopy experiments possess low frequency cutoffs of ∼2 THz (i.e., ∼8 meV). On the other hand, several theoretical works have studied the electronic structure of graphene in the direct vicinity of the Dirac point and predicted the existence of a finite density of states at the Dirac point in the presence of vacancies [9,10]. Such localized states at zero energy, also called midgap states, can act as charge traps and play an important role on the Fermi level position [11].

Here, we investigate the conductivity of MEG in the vicinity of the Dirac point using THz time-domain spectroscopy at temperatures ranging from 5 K to 300 K. We show that the properties of the quasineutral layers are well described by a Fermi level pinned at the Dirac point. We highlight that the dominant scattering mechanism close to the Dirac point is due to intrinsic midgap states, whereas at higher energy (>8 meV), scatterings on short-range potential introduced by residual intrinsic defects dominate, in agreement with previous reported works [12]. The midgap states introduced by intrinsic defects can be responsible for the pinning of the Fermi level at the Dirac point. This paper shows the potential of *THz time-domain spectroscopy as a function of temperature* for investigating the electronic and optical properties of graphene layer stacking very close to the Dirac point without the need of electrical contacts.

II. RESPONSE OF MULTILAYER GRAPHENE FROM $T = 5$ K TO $T = 300$ K

The THz time-domain spectroscopy experiment is based on 15 fs optical pulses at a central wavelength of 800 nm delivered by a mode-locked Ti:Sa laser with an 80 MHz repetition rate. A large-area interdigitated photoconductive antenna is used for THz pulse emission and a 100 μm thick GaP crystal for coherent detection [13]. The experiment extends from 0.4 THz to 4 THz with a spatial resolution limited by diffraction [14]. The graphene sample and a bare SiC substrate used as a reference are mounted in a cryostat with polyethylene windows. The MEG sample is produced by thermal desorption of Si from the C-terminated face of single-crystal 4H-SiC(000-1) [15] and contains typically a few tens of independent layers with non-Bernal rotated graphene planes. From magnetospectroscopy measurements, we find that the Fermi levels of the heavily-doped layers to be 360, 275, 130, and 80 meV above the Dirac point of the respective layers and the Fermi level of the quasineutral layers to be <7 meV above their Dirac point. The Fermi level of the first four heavily-doped layers near the substrate investigated in previous studies in similar MEG samples are very consistent with our findings [6].
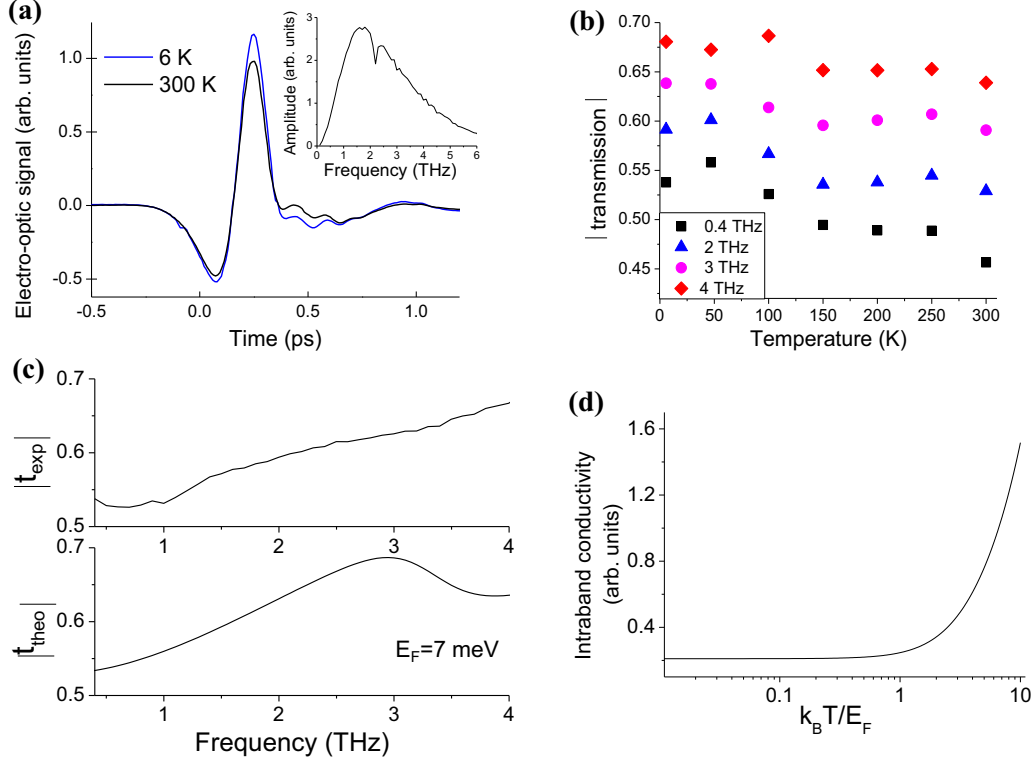
FIG. 1. (a) Transmitted THz electric field through the graphene sample at 5 K (blue) and 300 K (black). Insert: Corresponding amplitude spectrum of the THz electric field at $T = 300$ K obtained by fast Fourier transform. (b) Transmittance as a function of the temperature for different frequencies. (c) Amplitude transmittance spectrum $|t(\omega)|$ of the graphene multilayers at 5 K measured (top) and predicted (bottom) for $E_F = 7$ meV. (d) Calculation of the intraband conductivity in graphene as a function of $k_B T/E_F$ [16].

The transmitted THz waveforms through the graphene sample and the bare SiC substrate were measured from 5 K to 300 K, as illustrated in Fig. 1(a). Using Fourier transformation, the amplitude transmittance spectra $t(\omega)$ in the frequency domain from 0.4 THz to 4 THz was obtained. Figure 1(b) shows the transmittance as a function of the temperature for different frequencies. We clearly observe that the overall transmittance and thus the total conductivity strongly varies with temperature for all frequencies. These changes are due to the temperature-dependent conductivity of the quasineutral layers only. Indeed, the conductivity of the highly-doped layers, for which $\hbar\omega \ll 2E_F$, is governed by intraband transition processes. These processes are well described by a Drude model that neglects thermal broadening of the electron distribution since $E_F > k_B T$ [16]. Using this Drude model, the intraband transition processes in the highly-doped layers ($k_B T/E_F < 1$) are predicted to be independent of the temperature from 5 K to 300 K, as shown in Fig. 1(d). Thus, the temperature dependence of the transmittance observed in Fig. 1(b) results from the intraband and the interband conductivities of the quasineutral layers. Figure 1(c) (upper panel) shows the amplitude transmittance spectrum $|t(\omega)|$ of the multilayer graphene at 5 K. The transmittance is nearly constant up to 1 THz and then increases monotonously. We report in Fig. 1(c) (bottom panel) the calculated transmittance at 5 K of a multilayer graphene sample consisting of the four doped layers and $N_l = 53$ quasineutral layers of Fermi level $E_F = 7$ meV using our model described below. A negative slope in the transmittance is observed around 3.5 THz

corresponding to $f = 2E_F/h$ due to the establishment of the interband conductivity. Indeed, in graphene at low temperature, intraband (Drude) conductivity shows monotonic frequency dependence, whereas interband conductivity provides a sharp response around $2E_F$. The negative slope extends over more than 1 THz due to thermal smearing of the $2E_F$ feature [17]. It is surprising that such a slope change is not observed in the measured transmission spectra, as the build-up of the interband conductivity of the quasineutral layers is expected at $f < 3.5$ THz (i.e., $2E_F < 14$ meV). Two possibilities can explain this behavior. The first would be a broadening of the chemical potential in the quasineutral layers leading to a smooth interband response. However, the narrow width for the magnetotransmission line (involving Landau levels $L_{1(0)}$ and $L_{0(1)}$, respectively, in the valence and conduction bands) measured over a large area in MEG samples by magnetospectroscopy [here, see Fig. 3(a), and also in many previous works [5]] demonstrates the weak chemical potential fluctuations in the quasineutral layers. The second reason would be a Fermi level of the quasineutral layers lower than the investigated spectral range, i.e., $E_F \leqslant 1$ meV. This reason is supported by the change of the experimental transmission spectra as soon as the temperature is increased from its lowest value ($k_B T = 1$ meV at $T = 11$ K) considering that interband and intraband processes in graphene vary with temperature only for $E_F \leqslant k_B T$.

For a more thorough understanding of the interplay between interband and intraband processes in the quasineutral graphene layers, we perform a full calculation of the

temperature-dependent THz conductivity in the highly-doped and the quasineutral graphene layers. The transmitted field through the graphene sample normalized to the transmitted field through the substrate is related to the total conductivity of the graphene layers by

$$t(\omega) = \frac{1+n}{1+n+Z_0\sigma(\omega)},$$

where n is the refractive index of the SiC substrate, ω is the angular frequency, Z_0 is the free space impedance, and $\sigma(\omega)$ is the complex total conductivity of the graphene layers. The total conductivity includes the contribution of the four highly-doped layers $\sigma_{\mathrm{doped}}(\omega)$ and of the N_l quasineutral layers $\sigma_{\mathrm{QN}}(\omega)$ and is given by

$$\sigma(\omega) = \sigma_{\mathrm{doped}}(\omega) + N_l\sigma_{\mathrm{QN}}(\omega).$$

$\sigma_{\mathrm{doped}}(\omega)$ relies on intraband processes only as discussed earlier and is calculated using a scattering time of 70 fs, in agreement with a previous report [18]. The intraband and interband processes in the quasineutral layers compete at THz frequencies [19], and thus

$$\sigma_{\mathrm{QN}}(\omega) = \sigma_{\mathrm{QN\_inter}}(\omega) + \sigma_{\mathrm{QN\_intra}}(\omega).$$

For the intraband conductivity, the thermal broadening of the electron distribution must be taken into account since its magnitude is of the same order as the Fermi energy. Thus, we describe the frequency-dependent intraband conductivity of the thermalized electron gas in the quasineutral graphene layer using

$$\sigma_{\mathrm{QN\_intra}}(\omega) = -\frac{e^2 v_{\mathrm{F}}^2}{2} \int_{-\infty}^{+\infty} D(E) \frac{\tau(E)}{1-i\omega\tau(E)} \\ \times \frac{\partial f_{\mathrm{FD}}(\mu,T,E)}{\partial E} dE,$$

where $D(E) = \frac{2}{\pi\hbar^2 v_{\mathrm{F}}^2}|E|$ is the energy-dependent density of states in graphene, $\tau(E)$ is the electron momentum scattering time, v_F is the Fermi velocity, and f_{FD} the Fermi Dirac distribution [20]. $\mu(T)$ is the chemical potential that is a decreasing function of the temperature calculated considering the conservation of the total particle number in the system. The interband conductivity of one quasineutral graphene layer is given by

$$\sigma_{\mathrm{QN\_inter}}(\omega) = \frac{\pi e^2}{4h} \left[\tanh\left(\frac{\hbar\omega + 2\mu(T)}{4k_B T}\right) \\ + \tanh\left(\frac{\hbar\omega - 2\mu(T)}{4k_B T}\right) \right].$$

There are several possible sources of carrier scattering in graphene: short-range scattering on intrinsic defects, long-range scattering on Coulomb impurities, scattering on midgap states, phonon scattering, and carrier-carrier scattering. Previous studies on MEG have shown that the scattering time in the quasineutral layers is inversely proportional to the carrier energy and is dominated by short-range scattering on residual intrinsic defects over a very broad energy range from 10 meV to 1.5 eV [12,21]. Long-range scattering on Coulomb impurities

in the quasineutral layers can be neglected since the layers inside the stack are naturally protected and screened from the environment; the thermal decomposition growth process directly from the SiC substrate prevents contamination by extrinsic impurities. We do not consider in the model scattering mechanisms due to absorption of optical phonons since the thermal energy in this paper remains considerably lower than the optical phonon energy in graphene (200 meV). Finally, contributions due to interactions with acoustic phonons as well as carrier-carrier scattering are usually considered to be relatively small for low-energy carriers [22].

A. Scattering on short range potentials

The symbols in Fig. 2(a) show the transmission spectra measured at 5 K, 50 K, 100 K, 200 K, and 300 K from 0.4 to 4 THz. It is observed that from 5 K to 50 K, the transmission (absorption) slightly increases (decreases) over the entire spectral range, and above 50 K the absorption of the graphene layers increases as the temperature is increased. Below 1 THz, the transmission spectra are virtually flat except at a temperature of 300 K. Above 1 THz, the spectra show a monotonic behavior with the frequency. We also observe that the spectra at 4 K, 50 K, and 100 K overlap around 3.7 THz. In Fig. 2(b), the transmission spectra calculated using our model for $E_F = 0$ meV are reported, and in Fig. 2(c) the deviation from the calculated to experimental data expressed by $\Delta t = |t_{\mathrm{exp}}| - |t_{\mathrm{theo}}|$ is shown. The dashed lines in Fig. 2(b) and the black symbols in Fig. 2(c) are the calculated data considering carrier scattering on short-range potentials with a momentum scattering time given by $\tau_{\mathrm{SR}} = \alpha/|E|$, where α is a constant-temperature independent fit parameter ($\alpha = 1$ fs/eV and $N = 53$ layers have been used in the calculations). The model generally reproduces the measured data from 1.5 THz to 4 THz, indicating the main role played by scattering on short-range potentials, in agreement with previous reports [12]. However, a strong discrepancy between the predicted and measured transmission is observed at low frequency (below ~1.5 THz). Indeed, the deviation from calculated to experimental data reported in Fig. 2(c) increases continuously as the frequency is decreased below 1.5 THz to reach more than 10% at 0.4 THz for temperatures of 50 K, 100 K, and 200 K. Thus, our results reveal that an additional scattering mechanism is involved at energies close to the Dirac point.

B. Scattering on short-range potentials and mid-gap states

As is known, vacancies in graphene give rise to bound states at the Dirac point, the so-called midgap states [23]. Scattering by such defects may also be involved in the low-frequency intraband conductivity of the quasineutral layers. To incorporate their contribution in the model, we include the scattering time given by $\tau_{\mathrm{MD}} = \beta|E|(\ln\gamma E)^2$, with γ related to the radius of vacancies and where β is a constant-temperature independent fit parameter [24]. The total momentum scattering rate is thus given by $\Gamma = (\alpha/|E| + \beta|E|(\ln\gamma E)^2)^{-1}$. The solid lines in Fig. 2(b) show the transmission spectra calculated for $\alpha = 1$ fs/eV, $\beta = 20$ ps/eV, and $\gamma = 0.1$. One can see that our model based on scattering on both short-range potentials and on midgap states agree well with the experimental data
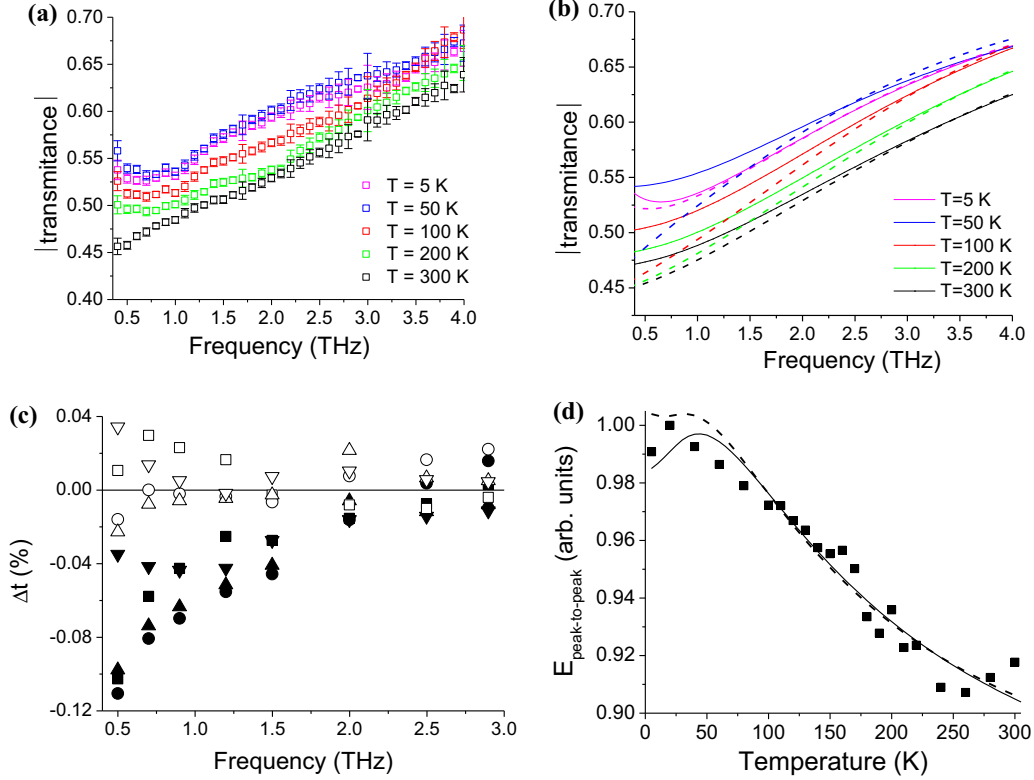
FIG. 2. (a) Experimental transmission spectra of MEG at 5 K, 50 K, 100 K, 200 K, and 300 K. The error bars are the standard deviation in the measurements. (b) Corresponding calculated transmission spectra of graphene layers considering scattering on short-range potentials only (dashed line) and considering both scattering on short-range potentials and on mid-gap states (solid line). (c) Deviation in percent from calculated to experimental data $\Delta t = |t_{\mathrm{exp}}| - |t_{\mathrm{theo}}|$ as a function of frequency. Black symbols result from calculations assuming scattering on short-range potentials only and open symbols on both scattering processes. (d) Peak-to-peak electric field transmitted through the graphene sample normalized to that of the SiC substrate as a function of temperature (symbols are experimental data; dashed and solid lines are the calculated data, assuming one and two scattering mechanisms, respectively).

for $E_F = 0$ meV. In particular, it reproduces the decrease of the transmission with increasing temperature, the monotonic frequency dependence above 1 THz, the plateau at lower frequencies, and also the overlap of the spectra at 4 K, 50 K, and 100 K around 3.7 THz. We estimate that our accuracy on the Fermi level is 1 meV (i.e., $2 E_F = 2$ meV) owing to the low cutoff frequency of the THz time-domain spectroscopy experiment. The role of midgap states in scattering mechanisms is also highlighted in Fig. 2(d), which reports the peak-to-peak electric field transmitted through the graphene sample normalized to that of the SiC substrate as a function of temperature with a resolution of 20 K [symbols in Fig. 2(d)]. Our model with $E_F = 0$ meV and the two scattering mechanisms (solid line) reproduces well the data, while a strong discrepancy below 100 K is observed when only scattering on short-range potentials (dashed line) is considered. These results strengthen our assumption on the position of the Fermi level in the quasineutral layers since midgap states can pin the Fermi level at the Dirac point [see Fig. 3(a)].

It is worth noting that by considering scattering on both short-range potentials and on Coulomb impurity (instead of midgap states), our model could also fit the data. Indeed, scattering time on long-range Coulomb potentials (caused by charged impurities in the substrate) is proportional to

the energy E and so differs from the scattering time on midgap states only by the logarithmic correction. However, as mentioned above, the random potential fluctuations in the quasineutral graphene layers caused by the charged impurities in the substrate are expected to be strongly suppressed due to both effects of environmental dielectric screening and distance from the SiC substrate. Indeed, graphene has remarkable nonlinear screening capability, and, for instance, it has been recently shown that the insertion of a single graphene buffer layer increases the carrier scattering time of a graphene layer by a factor of 2.3 [25]. Thus, the first four doped graphene layers in the MEG sample induce an important screening effect of the potential fluctuations caused by impurities in the substrate. In addition, it has been demonstrated that an increase of the distance of a graphene layer from the substrate reduces the strength of the potential fluctuations caused by the charged impurities in the substrate [26]. In return, vacancies responsible for scattering on midgap states are located within the quasineutral graphene layers. Thus, we expect that even if scattering on long-range Coulomb potentials is involved, carrier scattering on midgap states is the predominant scattering process at low energy.

Our paper provides a unique insight in the scattering mechanisms involved at energies close to the Dirac point. They
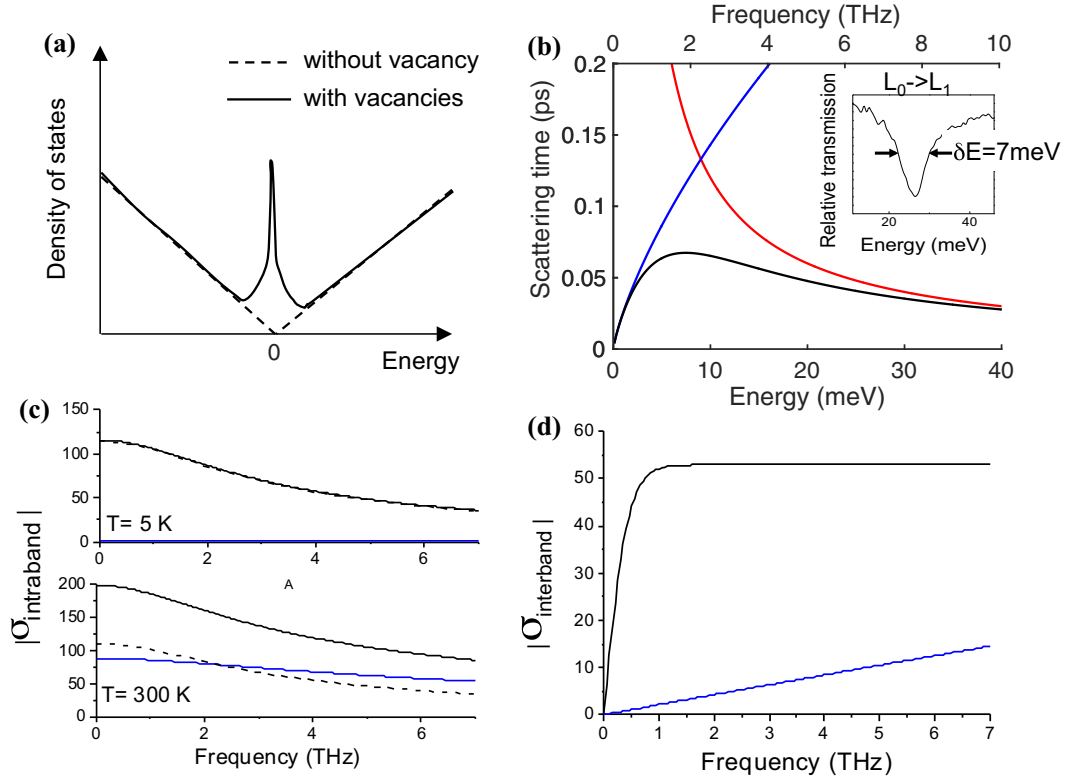
FIG. 3. (a) Schematic of the density of states of graphene without and with vacancies. (b) Scattering times as a function of carrier energies: scattering time on short-range potentials (red line), scattering time on channels related to the presence of vacancy defects (blue line), and the total scattering time including both scattering mechanisms (black line). (c) The predicted intraband conductivity of the quasineutral layers for $E_F = 0$ of the highly-doped layers and the total intraband conductivity at 5 K and 300 K. (d) The interband conductivity of the quasineutral layers at 5 K (blue line) and 300 K (black line).

result from the interplay between scattering on short-range potentials and on channels via midgap states related to the presence of vacancy defects. We show in Fig. 3(b) that carrier scattering is governed by the latter for $\hbar\omega < 8$ meV, whereas scattering on short-range potentials dominates at higher energies. We can furthermore compare the calculated total scattering time with the spectral broadening of inter-Landau-level transitions extracted from magnetospectroscopy measurements. The insert of Fig. 3(b) shows the measured spectrum, highlighting the inter-Landau-level $L_{1(0)} \rightarrow L_{0(1)}$ transitions for a magnetic field of 0.5 T. The transition energy is 26 meV, and its broadening (full width at half maximum) is ∼7 meV, corresponding to a carrier scattering time of $\tau = \hbar/\Gamma = 94$ fs. This value is ∼2 times higher than the scattering time extracted from our analysis. This discrepancy may originate from the reduction of scattering processes when a magnetic field is applied due to the localization of carriers.

A further interesting aspect of our paper in temperature is the identification of the distinct conductivities in the highly-doped layers and in the quasineutral layers. Figure 3(c) shows the predicted intraband conductivity of the quasineutral layers for $E_F = 0$ meV and of the highly-doped layers at 5 K and 300 K. The intraband conductivity of the highly-doped layers is constant from 5 K to 300 K, as expected, and dominates the total intraband conductivity of MEG at low temperature. Conversely at 300 K, the contribution of intraband conductivity from quasineutral layers is strongly

increased from 5 K to 300 K owing to the thermal distribution of electron. The interband conductivity of the quasineutral layers, shown in Fig. 3(d), follows the standard evolution of thermal electronic distribution [27]. Our analysis demonstrates interband transitions in MEG at THz frequencies. This opens the route to the development of graphene-based devices for THz photonic applications such as saturable absorbers.

III. CONCLUSION

In conclusion, we have investigated the THz conductivity of MEG from 5 K to 300 K and show that the properties of the quasineutral layers are well described by a Fermi level pinned at the Dirac point by midgap states. We highlight that the dominant scattering mechanisms are a result of intrinsic defects that induce scatterings on short-range potentials and midgap states [12]. THz time-domain spectroscopy as a function of temperature is revealed as a powerful technique for investigating the electronic and optical properties close to the Dirac point of two-dimensional based materials without the need of contact. Furthermore, these findings show the potential of MEG for probing the properties of Dirac particles close to the Dirac point but also for THz photonic devices that rely on interband processes at THz frequencies.

[1] A. Tredicucci and M. S. Vitiello, Device, IEEE J. Sel. Topics Quantum Electron. **20**, 130 (2014).

[2] L. Ren, Q. Zhang, J. Yao, Z. Sun, R. Kaneko, Z. Yan, S. Nanot, Z. Jin, I. Kawayama, M. Tonouchi, J. M. Tour, and J. Kono, Nano Lett. **12**, 3711 (2012).

[3] C. Berger, Z. Song, X. Li, X. Wu, N. Brown, C. Naud, D. Mayou, T. Li, J. Hass, A. N. Marchenkov, E. H. Conrad, P. N. First, and W. A. de Heer, Science **312**, 1191 (2006).

[4] M. Sprinkle, D. Siegel, Y. Hu, J. Hicks, A. Tejeda, A. Taleb-Ibrahimi, P. Le Fèvre, F. Bertran, S. Vizzini, H. Enriquez, S. Chiang, P. Soukiassian, C. Berger, W. A. de Heer, A. Lanzara, and E. H. Conrad, Phys. Rev. Lett. **103**, 226803 (2009).

[5] M. Orlita, C. Faugeras, P. Plochocka, P. Neugebauer, G. Martinez, D. K. Maude, A.-L. Barra, M. Sprinkle, C. Berger, W. A. de Heer, and M. Potemski, Phys. Rev. Lett. **101**, 267601 (2008).

[6] D. Sun, C. Divin, C. Berger, W. A. de Heer, P. N. First, and T. B. Norris, Phys. Rev. Lett. **104**, 136802 (2010).

[7] M. Mittendor, F. Wendler, E. Malic, A. Knorr, M. Orlita, M. Potemski, C. Berger, W. A. de Heer, H. Schneider, Ma. Helm, and S. Winnerl, Nature Physics **11**, 75 (2015).

[8] Y.-M. Lin, C. Dimitrakopoulos, D. B. Farmer, S.-J. Han, Y. Wu, W. Zhu, D. K.Gaskill, J. L. Tedesco, R. L. Myers-Ward, C. R. Eddy, Jr., A. Grill, and P. Avouris, App. Phys. Lett. **97**, 112107 (2010).

[9] N. M. R. Peres, F. Guinea, and A. H. Castro Neto, Phys. Rev. B **73**, 125411 (2006).

[10] V. M. Pereira, J. M. B. Lopes dos Santos, and A. H. Castro Neto, Phys. Rev. B **77**, 115109 (2008).

[11] Z. Moktadir, S. Hang, and H. Mizuta, Carbon **93**, 325 (2015).

[12] M. Orlita, C. Faugeras, R. Grill, A. Wysmolek, W. Strupinski, C. Berger, W. A. de Heer, G. Martinez, and M. Potemski, Phys. Rev. Lett. **107**, 216603 (2011).

[13] Y. S. Lee, *Principles of THz Science and Technology* (Springer, New York, 2009), Chap. 3.

[14] M. Baillergeau, K. Maussang, T. Nirrengarten, J. Palomo, L. H. Li, E. H. Linfield, A. G. Davies, S. Dhillon, J. Tignon, and J. Mangeney, Scientific Reports **6**, 24811 (2016).

[15] W. A. de Heer, C. Berger, M. Ruan, M. Sprinkle, X. Li, Y. Hu, B. Zhang, J. Hankinson, and E. Conrad, Proc. Natl. Acad. Sci. USA **108**, 16900 (2011).

[16] A. J. Frenzel, C. H. Lui, Y. C. Shin, J. Kong, and N. Gedik, Phys. Rev. Lett. **113**, 056602 (2014).

[17] Z. Q. Li, E. A. Henriksen, Z. Jiang, Z. Hao, M. C. Martin, P. Kim, H. L. Stormer, and D. N. Basov, Nat. Phys. **4**, 532 (2008).

[18] I. Crassee, M. Orlita, M. Potemski, A. L. Walter, M. Ostler, Th. Seyller, I. Gaponenko, J. Chen, and A. B. Kuzmenko, Nano Lett. **12**, 2470 (2012).

[19] S. Winnerl, M. Orlita, P. Plochocka, P. Kossacki, M. Potemski, T. Winzer, E. Malic, A. Knorr, M. Sprinkle, C. Berger, W. A. de Heer, H. Schneider, and M. Helm, Phys. Rev. Lett. **107**, 237401 (2011)

[20] Z. Mics, K.-J. Tielrooij, K. Parvez, S. A. Jensen, I. Ivanov, X. Feng, K. Mullen, M. Bonn, and D. Turchinovich, Nat. Commun. **6**, 7655 (2015).

[21] M. T. Mihnev, F. Kadi, C. J. Divin, T. Winzer, S. Lee, C.-H. Liu, Z. Zhong, C. Berger, W. A. de Heer, E. Malic, A. Knorr, and T. B. Norris, Nat. Commun. **7**, 11617 (2016).

[22] T. Stauber, N. M. R. Peres, and F. Guinea, Phys. Rev. B **76**, 205423 (2007).

[23] S. Das Sarma, S. Adam, E. H. Hwang, and E. Rossi, Rev. Mod. Phys. **83**, 407 (2011).

[24] T. O. Wehling, S. Yuan, A. I. Lichtenstein, A. K. Geim, and M. I. Katsnelson, Phys. Rev. Lett. **105**, 056802 (2010).

[25] C.-P. Lu, M. Rodriguez-Vegab, G. Lia, A. Luican-Mayera, K. Watanabec, T. Taniguchic, E. Rossi, and E. Y. Andreia, PNAS **113**, 6623 (2016)

[26] S.-Z. Liang, G. Chen, A. R. Harutyunyan, and J. O. Sofo, Phys. Rev. B **90**, 115410 (2014).

[27] K. F. Mak, M. Y. Sfeir, Y. Wu, C. H. Lui, J. A. Misewich, and T. F. Heinz, Phys. Rev. Lett. **101**, 196405 (2008).